DISCOVERY OF A DISSOCIATIVE GALAXY CLUSTER MERGER WITH LARGE PHYSICAL SEPARATION

William A. Dawson[1], David Wittman[1], M. James Jee[1], Perry Gee[1], John P. Hughes[2], J. Anthony Tyson[1], Samuel Schmidt[1], Paul Thorman[1], Maruša Bradač[1], Satoshi Miyazaki[3], Brian Lemaux[1], Yousuke Utsumi[3], Vera E. Margoniner[4]

Draft version February 21, 2012

ABSTRACT

We present DLSCL J0916.2+2951 (z=0.53), a newly discovered major cluster merger in which the collisional cluster gas has become dissociated from the collisionless galaxies and dark matter. We identified the cluster using optical and weak lensing observations as part of the Deep Lens Survey. Our follow-up observations with *Keck*, *Subaru*, *Hubble Space Telescope*, and *Chandra* show that the cluster is a dissociative merger and constrain the dark matter self-interaction cross-section $\sigma_{\rm DM} m_{\rm DM}^{-1} \lesssim 7\,{\rm cm}^2\,{\rm g}^{-1}$. The system is observed at least $0.7 \pm 0.2\,{\rm Gyr}$ since first pass-through, thus providing a picture of cluster mergers 2–5 times further progressed than similar systems observed to date. This improved temporal leverage has implications for our understanding of merging clusters and their impact on galaxy evolution.

Subject headings: cosmic background radiation—dark matter—galaxies: clusters: individual (DLSCL J0916.2+2951)—gravitational lensing: weak—X-rays: galaxies: clusters

1. INTRODUCTION

During a major galaxy cluster merger the collisionless dark matter (DM) and galaxies become dissociated from the cluster gas (the principal baryonic component), a process that is observable for $\sim$2 Gyr (Ricker & Sarazin 2001). These mergers have become important astrophysical probes providing a diagnostic of large scale structure (LSS) formation, empirical evidence favoring DM over modified gravity (Clowe et al. 2006), constraints on the DM self-interaction cross-section (Markevitch et al. 2004), and constraints on the large scale matter-antimatter ratio (Steigman 2008). They are also a suspected source of extremely energetic cosmic rays (van Weeren et al. 2010). A special subclass of mergers are probes of all the aforementioned science. Such mergers: 1) are between two subclusters of comparable mass, 2) have a small impact parameter, 3) are observed during the short period when the cluster gas is significantly offset from the galaxies and DM, and 4) occur mostly transverse to the line-of-sight so that the apparent angular separation of the cluster gas from the galaxies and DM is maximized. We term these systems *dissociative mergers*. Given these requirements it is not surprising that only six such systems have been confirmed: 1E 0657-56 (Clowe et al. 2006), MACS J0025.4-1222 (Bradač et al. 2008), Abell 520 (Mahdavi et al. 2007; Okabe & Umetsu 2008), Abell 2744 (Merten et al. 2011), Abell 2163 (Okabe et al. 2011), and Abell 1758 (Ragozzine et al. 2011). With such a small sample which only probes a narrow temporal window ($\sim$0.17–0.25 Gyr

post-collision[5]), it is not surprising that we still do not completely understand merging systems. For example, Mahdavi et al. (2007) and Jee et al. (2012, ApJ, in press) find a "DM core" coincident with X-rays but not with any bright cluster galaxies in the merging system A520, and Merten et al. (2011) find a "ghost" clump of gas leading a DM clump in A2744; there is no accepted explanation for either of these observations. Simulations are needed to provide insight into these mysteries, but hydrodynamic simulations are complex and many assumptions are required (see e.g. Springel & Farrar 2007; Poole et al. 2006): therefore observations of new and different systems will play a crucial role in building confidence in these simulations.

We have identified a new dissociative merger, DLSCL J0916.2+2951, that probes an unexplored area of merger phase-space. We originally detected the cluster in the Deep Lens Survey (DLS; Wittman et al. 2002) via its weak lensing (WL) shear signal. It consists of two main subclusters spectroscopically confirmed to be at the same redshift (0.53). This cluster was also observed in the Sunyaev-Zel'dovich Array Survey (Muchovej et al. 2011) which provided evidence that the cluster gas is dissociated from the bulk of the mass and galaxies. Follow-up optical observations with *Subaru* and *HST* enable higher resolution mass maps and follow-up X-ray observations with *Chandra* ACIS-I confirm that the majority of the gas is offset between the North and South subclusters, the signature of a dissociative merger (Figure 1).

In this letter we introduce DLSCL J0916.2+2951 and summarize our survey of its three dominant components (galaxies, DM, and gas) and the cluster's astrophysical implications. A more thorough exposition of the survey and analysis will be presented in Dawson et al. (in preparation). Throughout this paper we assume $\Omega_\Lambda = 0.7$, $\Omega_m = 0.3$, and $H = 70\,{\rm km\,s}^{-1}\,{\rm Mpc}^{-1}$.

wadawson@ucdavis.edu

[1] University of California, Davis, Physics Department, One Shields Av., Davis, CA 95616, USA
[2] Department of Physics and Astronomy, Rutgers University, 136 Frelinghuysen Road, Piscataway, NJ 08854-8019, USA
[3] Department of Astronomical Science, The Graduate University for Advanced Studies, 2-21-1 Osawa, Mitaka, Tokyo 181-8588, Japan
[4] Department of Physics and Astronomy, California State University, Sacramento, 6000 J Street Sacramento, CA 95819, USA

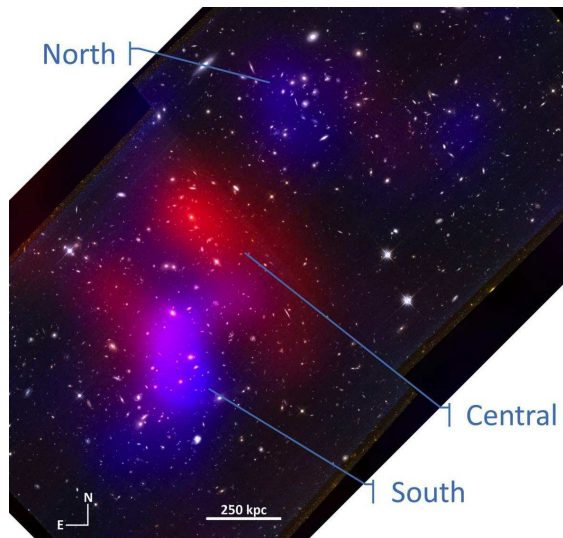[5] We define the time of collision to be the time of the first pericentric passage.

FIG. 1.— Merging cluster DLSCL J0916.2+2951 and its three matter components. Overlaid on the HST color image of the galaxies is the total mass distribution (blue) based on WL analysis of the HST images and the cluster gas distribution (red) based on Chandra X-ray observations. The bulk of the collisional gas is located between the two collisionless galaxy and mass concentrations, indicative of a dissociative merger. The image is $5' \times 5'$ ($\sim 1.9 \times 1.9 \, \mathrm{Mpc}^2$ at $z = 0.53$).

2. OPTICAL ANALYSIS

We obtained spectroscopic redshifts for 20 cluster members with *Keck* LRIS (2007 January 16) and 634 unique spectroscopic redshifts ($0 < z < 1.2$) in a $\sim 15' \times 15'$ area centered on the cluster with *Keck* DEIMOS (2011 March 2–3), including 132 members at the cluster redshift. We reduced the LRIS spectra using a scripted sequence of standard IRAF reduction tasks, and the DEIMOS spectra using a modified version of the DEEP2 *spec2d* package (Davis et al. 2003; Gal et al. 2008; Lemaux et al. 2009).

We use our full sample of 654 spectroscopic redshifts as well as photometric redshifts to identify potential line-of-sight structures which may confuse our results. We find no evidence for significant line-of-sight structure (Figure 2).

We estimate each subcluster's redshift and velocity dispersion (Table 1) using the biweight-statistic and bias-corrected 68% confidence limit (Beers et al. 1990) applied to 100,000 bootstrap samples of each subcluster's spectroscopic redshifts. Our redshift estimates indicate a line-of-sight velocity difference of $v_{\mathrm{los}} = 670^{+270}_{-330}$ km s^{-1} between the North and South subclusters, using the galaxies within a 0.5 Mpc radius centered on the *HST* WL mass peaks and within a velocity range of $\pm 3000 \, \mathrm{km \, s^{-1}}$ of z=0.53 ($\sim 3\times$ the expected velocity dispersion); corresponding to 38 and 35 galaxies for the North and South subclusters, respectively. These results are robust against varying the velocity range $\pm 1000 \, \mathrm{km \, s^{-1}}$ and using the Subaru WL or galaxy number density peaks as the apertures' centers, provided the aperture radius is $\lesssim 0.5 \, \mathrm{Mpc}$: larger radii lead to significant subcluster membership confusion. Additionally, we report the velocity dispersion mass estimates based on the scaling relation of Evrard et al. (2008) in Table 1.

We obtained B, V, R, and z' photometric data (12, 12, 18, and 12 ksec, respectively) with Mosaic 1 on the

KPNO 4-m *Mayall* telescope as part of the DLS. To improve the accuracy of our photometric redshifts we also observed the cluster in three medium-width optical bands ($g, h,$ and i from the BATC filter set), bracketing the redshifted 4000 Å feature, using the upgraded Mosaic 1.1 imager on the KPNO *Mayall* with exposure times of 6 ks per filter (2011 April 22–24). We estimate colors using *ColorPro* (Coe et al. 2006) and redshifts using *BPZ* (Benítez 2000). We replace the standard templates with a set "tweaked" in a method similar to that described in Ilbert et al. (2006), using spectroscopic samples from SHELS (Geller et al. 2005) and the PRIMUS survey (Coil et al. 2010) which overlap the DLS. Figure 2 shows the density isopleths of galaxies with $0.43 < z_{\mathrm{phot}} < 0.63$ (roughly the cluster redshift $\pm \sigma_{z_{\mathrm{phot}}}$). This map agrees well with the distribution of spectroscopically confirmed cluster members.

3. WEAK LENSING ANALYSIS

To map the total mass distribution we use a version of the Fischer & Tyson (1997) method modified to include a novel tomographic signal-matched filter. The cluster's WL shear signal, γ, depends not only on the projected surface mass over-density of the cluster, $\Delta\Sigma$, but on the relative distances of the observer, the mass, and the background galaxies:

$$\gamma = \frac{\Delta\Sigma}{\Sigma_{cr}} = \frac{\Delta\Sigma 4\pi G}{c^2} \frac{D_{ls}(z_l, z_s) D_l(z_l)}{D_s(z_s)} \mathcal{H}\left(\frac{z_s}{z_l} - 1\right),$$

where Σ_{cr} is the critical surface density, $\mathcal{H}$ is the Heaviside step function, and D_l, D_s, & D_{ls} are the angular diameter distances to the lens, source, and between the lens and source, respectively. Since we do not have exact redshift measurements of the source galaxies we use each galaxy's photometric redshift probability distribution function, $p(z)$, to estimate a respective Σ_{cr} for a given lens redshift,

$$\Sigma_{cr}(z_l) \approx \langle \Sigma_{cr}(z_l) \rangle = \int \Sigma_{cr}(z_l, z_s) p(z_s) dz_s.$$

In addition to weights based on shape measurement errors, we also weight the shear of each galaxy based on its $p(z)$,

$$w_\gamma(z_l) = \frac{1}{\int \left[\Sigma_{cr}(z_l, z_s) - \langle \Sigma_{cr}(z_l) \rangle\right]^2 p(z_s) dz_s}.$$

This method increases the signal-to-noise of the measurement (see e.g. Hennawi & Spergel 2005), and more accurately accounts for the errors inherent in the photometric redshift estimates, compared to single-point estimates. We estimate uncertainties using 100 bootstrap resamplings.

Encouraged by the DLS mass and galaxy maps we obtained higher-resolution ground and space based observations. *Subaru* Suprime-Cam i'-band coverage of the cluster was provided by engineering-time observations of DLS Field 2 (2008 January 8). We use the Suprime-Cam data reduction software *SDFRED* (Yagi et al. 2002; Ouchi et al. 2004) followed by *SCAMP* & *SWARP* (Bertin et al. 2002; Bertin 2006) to refine the astrometry and make the final mosaic. DLSCL J0916.2+2951 was also observed with *HST* ACS/WFC using F606W
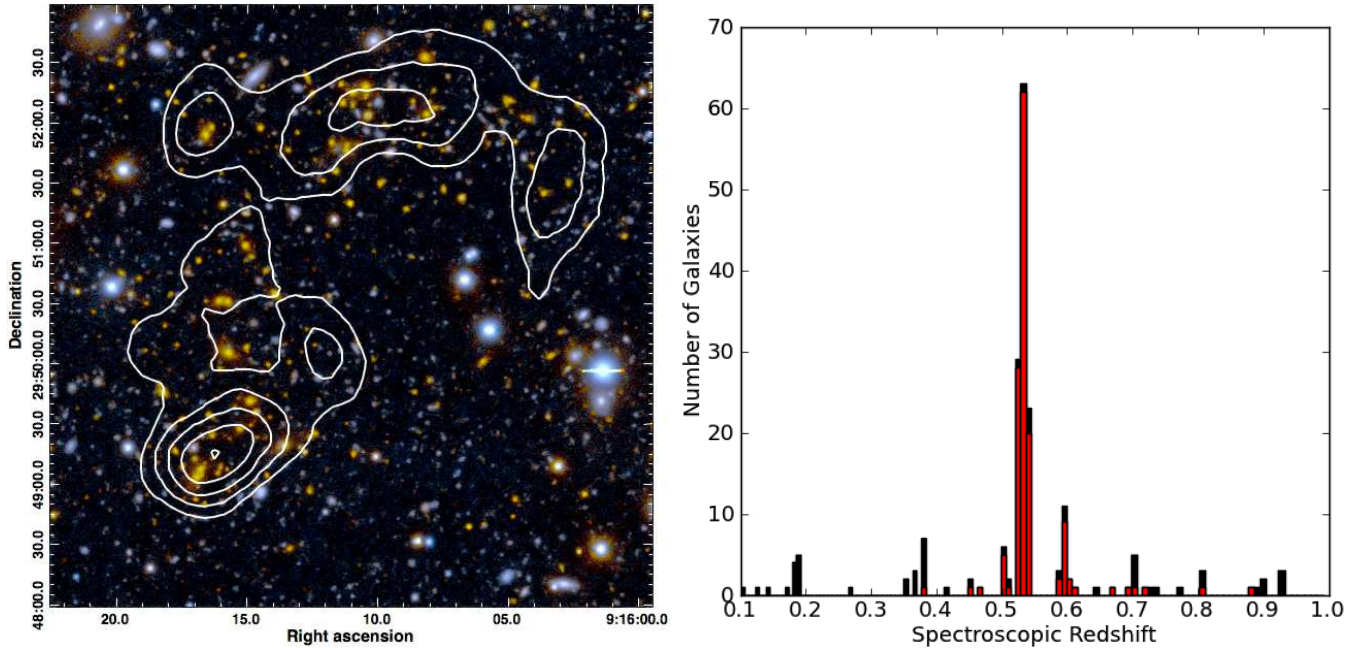
FIG. 2.— *Left:* DLS composite BVR color image of DLSCL J0916.2+2951 showing the galaxies of the two subclusters. The white contours represent the number density of galaxies with $z_{\rm phot} = 0.53 \pm 0.1$, the cluster redshift $\pm\sigma_{z_{\rm phot}}$. The contours begin at 200 galaxies $\rm Mpc^{-2}$ with increments of 50 galaxies $\rm Mpc^{-2}$. The image field-of-view is the same as Figure 1. *Right:* Histogram of the 200 observed spectroscopic redshifts within the field of view of the *left* figure. The red portion is the subsample that passes the $z_{\rm phot} = 0.53 \pm 0.1$ criteria. The galaxies at $z \sim 0.6$ had equal probability of selection as the cluster members and show no sign of clustering.

and F814W filters (GO-12377, PI-W. Dawson) in a 2×1 pointing mosaic that covers the subclusters (Figure 1). The exposure times for F606W and F814W are 2520s and 4947s per pointing, respectively. We reduce this data following a method similar to that presented in Jee & Tyson (2009). We measure the PSF of both datasets using the PCA method presented in Jee et al. (2007).

We perform our WL analysis independently on both the Subaru and HST F814W data. The Subaru data has $0.72''$ seeing and 49 WL-quality source galaxies (i.e. background galaxies with measured ellipticity error < 0.3) per arcmin^2. For the mass map we use an apodizing kernel radius of $0.5'$, which can be interpreted as the effective resolution of the WL mass map. We are able to cross-match most of the detected objects with the DLS and use the $p(z)$'s discussed in the previous section.

Cross-matching is more problematic with the higher-resolution HST data, so we use a color-magnitude cut (F606W-F814W < 0.8 and $24 <$ F814W < 28.5) to select source galaxies and exclude cluster red-sequence and bright foreground galaxies. For the WL analysis of the HST F814W image, which has a $0.1''$ PSF and 136 WL-quality source galaxies per arcmin^2, we use an apodizing kernel radius of $3.6''$. We find no significant spatial correlation between source density and subcluster position, suggesting that our source galaxy population is not significantly contaminated with cluster galaxies. We estimate the $p(z)$ of our HST source galaxy sample by assuming the photometric redshift distribution of the Coe et al. (2006) HUDF catalog after applying our color-magnitude cut. Figure 3 shows general agreement between the Subaru and HST WL mass, and galaxy density maps.

We construct a joint catalog from the HST and Subaru data, using the HST data where available and Sub-

aru for the surrounding area. Using a tomography-based MCMC analysis we simultaneously fit NFW halos centered on the North and South HST WL peaks, and use the Gelman & Rubin (1992) convergence test applied to eight independent chains. In order to reduce the number of free parameters we use the Duffy et al. (2008) empirical relation between M_{200} and concentration. We present the most likely masses for each halo along with the bias-corrected 68% confidence limits in Table 1. We also compare the integrated projected surface mass density of the NFW halos with the measured WL aperture mass (Fahlman et al. 1994) of each subcluster and find general agreement within a radius of 0.5 Mpc of each subcluster.

4. X-RAY ANALYSIS

We acquired X-ray spectral-imaging of the cluster with 40ks of *Chandra* ACIS-I time (GO-12800854), and reduce it using *CIAO* version 4.2 and *CALDB* version 4.4.1. We manually identify X-ray point sources and mask them before adaptively smoothing the diffuse emission, we present the resulting map in Figure 3. We estimate source counts and their error using the *dmextract* function of *CIAO*. We use an $8'$ radius background region which encloses the subcluster regions and rests $\sim 90\%$ on ACIS-I3 (on which the subclusters are observed); yet excludes subcluster, chip gaps, and point sources. For the South and Central X-ray concentrations (120 ± 17 and 170 ± 19 detected 0.5-2 keV photons, respectively) we use the *Xspec* X-ray spectral fitting tool (Arnaud 1996) to fit a Mewe-Kaastra-Liedahl plus photoelectric absorption model (fixed to the Leiden/Argentine/Bonn value; Kalberla et al. 2005) to the X-ray spectrum of each X-ray concentration. For the North concentration there are not enough detected X-ray photons (38 ± 12) to fit a meaningful spectrum. We report the results of this analysis in Table 1.
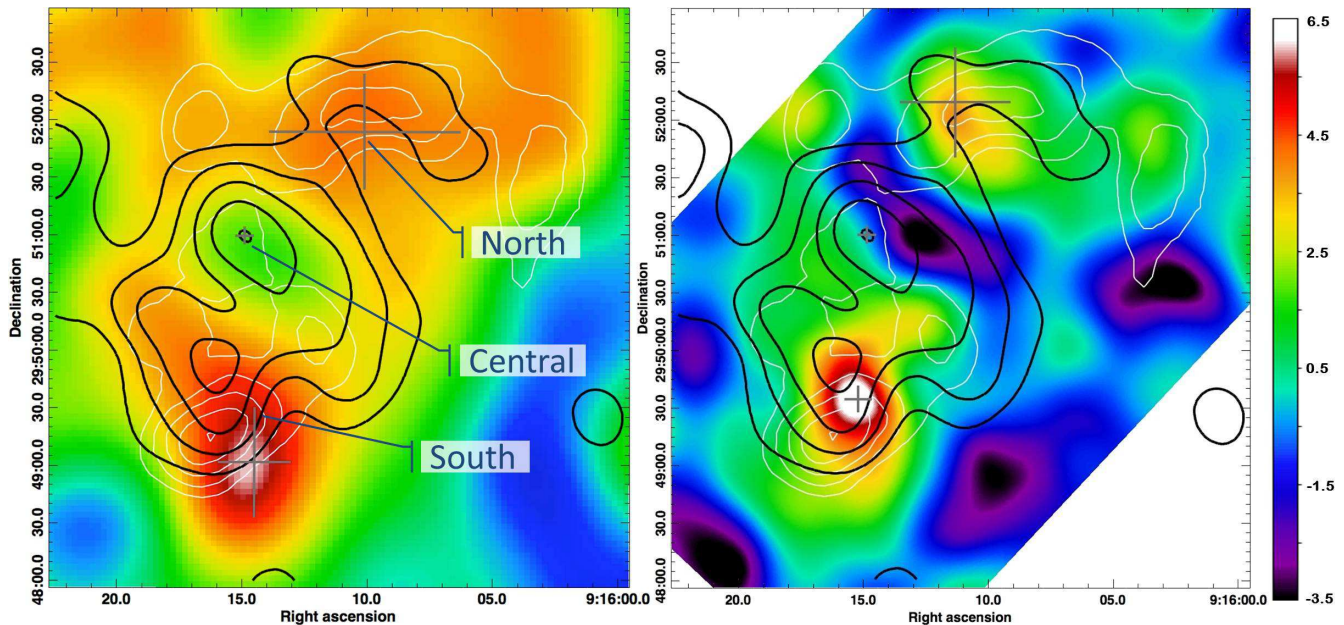
FIG. 3.— Comparison of the Subaru i'-band ground-based (left) and HST space-based (right) WL mass signal-to-noise maps (color) of DLSCL J0916.2+2951 with the X-ray distribution (bold black contours) and galaxy number density (white contours, same as Figure 2). The peak centers and corresponding one sigma errors are denoted by the gray cross-hairs. In both analyses there is general agreement between the location and relative magnitude of galaxies and WL yet the majority of the cluster gas is centered $\sim 1.4'$ between the North and South subclusters in a local mass underdensity, providing evidence that the North and South subclusters have undergone the first pass-through of a major merger. The scale of each map is equivalent and the image field-of-view is the same as Figures 1 & 2. The map created from the joint Subaru/HST catalog looks nearly identical to the HST map, with only slight variations in the scale (see Table 1).

5. CLUSTER MERGER SCENARIO

The peak of the gas distribution ($09^{\rm h}16^{\rm m}15^{\rm s} \pm 5.5^{\rm s}, 29°50'59'' \pm 5.0''$) derived from X-rays is offset $1.4' \pm 0.49$ from the North HST WL mass peak ($09^{\rm h}16^{\rm m}10^{\rm s} \pm 30^{\rm s}, 29°52'10'' \pm 30''$), and $1.4' \pm 0.14$ from the South HST WL mass peak ($09^{\rm h}16^{\rm m}15^{\rm s} \pm 8.0^{\rm s}, 29°49'34'' \pm 6.9''$), and is located near a local minimum in the mass, suggesting that the subclusters have a small impact parameter and have experienced at least their first pass-through along a north-northwest merger direction (see Figure 3). Further evidence for the merger scenario is provided by the morphology of the gas. Simulations (Schindler & Mueller 1993; Poole et al. 2006) predict that the gas morphology elongates transverse to the merger direction after pass-through for mergers with small impact parameters. The Central gas concentration appears to be oblate and roughly perpendicular to the axis connecting the North and South mass peaks. This is consistent with the interpretation that these two subclusters have experienced their first pass-through and that the merger axis being roughly in the plane of the sky.

We gain further insight into the dynamics of the system by studying the spectroscopic redshifts of the subcluster galaxies. The observed line-of-sight velocity difference, $v_{\rm los}(t_{\rm observed}) = 670^{+270}_{-330}$ km s^{-1}, between the North and South subclusters does not explicitly determine the dynamics or orientation of the system since there is a degeneracy between the three-dimensional relative peculiar velocity, $v_{\rm relative}$, and angle of the pair with respect to the plane of the sky, α. In order to constrain this degeneracy we perform a Monte Carlo analysis of the system assuming the clusters to be uniform-density spheres with R_{200} radii. We draw randomly from each subcluster's mass probability distribution as

determined by the NFW MCMC analysis, the redshift distribution of the spectroscopic bootstrap analysis, and the centroid distribution as determined by the bootstrap sample of the HST WL mass map. From these parameters we calculate a conservative upper bound on the relative velocity at the time-of-collision, $v_{\rm relative}(t_{\rm collision})$, by assuming that the two subclusters freely fell from an infinite separation and zero relative velocity yet began with their current mass. To determine a conservative lower bound we calculate $v_{\rm relative}(t_{\rm collision})$ assuming the subclusters had reached their observed separation with $v_{\rm relative}(t_{\rm observed}) = 0$. Implicit in our analysis is that the merger occurs with an impact parameter of zero. Including a moderate impact parameter of $\sim 0.1 R_{200}$ should have less than a 1% effect on the merger velocity (Mastropietro & Burkert 2008). As can be seen from Figure 4 the derived time-since-collision is relatively insensitive to moderate changes in $v_{\rm relative}(t_{\rm collision})$. For a consistency check we compare our analytic estimate of the Bullet Cluster's time-since-collision with the numerical model results of Springel & Farrar (2007) and find agreement within 20% (compare the square and diamond points of Figure 4). While we attempt to be conservative in our analysis, we disregard many complexities of the merger. Further insight will require deeper X-ray observations and/or hydrodynamic numerical simulations.

Using our analytic model we calculate that $v_{\rm relative}(t_{\rm collision}) = 1700^{+220}_{-280}$ km s^{-1}; given the sound speed of the gas ~ 600 km s^{-1}, this corresponds to a Mach number of ~ 3. With a projected separation of $1.0^{+0.11}_{-0.14}$ Mpc and estimated $\alpha = 34^{+20}_{-14}$ degrees we find a physical separation of $1.3^{+0.97}_{-0.18}$ Mpc between the North and South subclusters. This is the largest physical offset for a dissociative merger observed

TABLE 1
Observed subcluster and X-ray concentration properties

Subcluster	Redshift	σ_v (km s^{-1})	σ_v M$_{200}$ (10^{14}M$_\odot$)	WL M$_{200}$ (10^{14}M$_\odot$)	L$_{X_{0.5-2\mathrm{keV}}}$ (10^{43}erg s^{-1})	T$_X$ (keV)	X-ray S/N	Joint WL S/N
North	$0.53074^{+0.00068}_{-0.00064}$	740^{+130}_{-190}	3.7 ± 2.3	$1.7^{+2.0}_{-0.72}$	0.63	$\cdots$	3.2	3.0
South	$0.53414^{+0.00065}_{-0.00064}$	770^{+110}_{-92}	4.1 ± 1.6	$3.1^{+1.2}_{-0.79}$	2.1	$2.7^{+1.2}_{-0.7}$	7.0	6.7
Central	$\cdots$	$\cdots$	$\cdots$	$\cdots$	2.8	$2.2^{+1.4}_{-0.6}$	9.1	-3.3[a]

[a] The negative WL S/N indicates a projected surface mass local under-density.

to date. This translates into a time-since-collision ($t_{\mathrm{observed}} - t_{\mathrm{collision}}$) of $0.7^{+0.2}_{-0.1}$ Gyr. Given the collision velocities of the other dissociative mergers (Bradač et al. 2008; Markevitch et al. 2005; Springel & Farrar 2007; Merten et al. 2011) we calculate their times-since-collision using our analytic model and find that DLSCL J0916.2+2951 is probing a merger stage $\gtrsim 2 - 5$ times further progressed than any other known dissociative merger (Figure 4).

6. DARK MATTER IMPLICATIONS

Given the evident merger scenario we are able to use the first method of Markevitch et al. (2004) and place a rough limit on the DM self-interaction cross-section, σ_{DM}. This method compares the scattering depth of the dark matter, $\tau_{\mathrm{DM}} = \sigma_{\mathrm{DM}} m_{\mathrm{DM}}^{-1} \Sigma_{\mathrm{DM}}$, with that of the ICM gas, $\tau_{\mathrm{ICM}} \approx 1$, where m_{DM} is the DM particle mass and Σ_{DM} is the surface mass density of the DM particles. Σ_{DM} is approximately the WL measured surface mass density, Σ, since $\sim 80\%$ of a typical cluster's mass is DM (Diaferio et al. 2008). For ease of comparison with the results of Markevitch et al. (2004) and Merten et al. (2011) we examine the surface density averaged over the face of the subcluster within $r=125$ kpc, which is $\Sigma \approx 0.15\,\mathrm{g\,cm}^{-2}$; thus we find $\sigma_{\mathrm{DM}} m_{\mathrm{DM}}^{-1} \lesssim 7\,\mathrm{cm}^2\,\mathrm{g}^{-1}$. Note that we cannot apply the velocity-dependent σ_{DM} constraint methods outlined by Markevitch et al. (2004) since our analytic model assumes $\sigma_{\mathrm{DM}} = 0$.

7. DISCUSSION

While we use DLSCL J0916.2+2951 to provide further evidence for the canonical DM model and independently constrain $\sigma_{\mathrm{DM}} m_{\mathrm{DM}}^{-1}$, we believe that its greatest value is as a probe for a new and special phase of cluster formation. It provides a greatly improved temporal lever-arm with which to guide numerical simulations that explore the major merger phase. This is potentially important given that much of our knowledge of the cluster merger process comes from numerical hydrodynamic simulations (e.g. Poole et al. 2006), which are used to place the tightest constraints on $\sigma_{\mathrm{DM}} m_{\mathrm{DM}}^{-1}$ ($< 0.7\,\mathrm{cm}^2\,\mathrm{g}^{-1}$; Randall et al. 2008) and bring observed merger velocities (inferred from the observed shock velocity) more in line with the expectations of ΛCDM (Springel & Farrar 2007; Lee & Komatsu 2010). Secondly, the large projected separation relative to the virial radii of the subclusters ($R_{200} \sim 1$Mpc) enables the deconvolution of the subclusters from the Central region and direct comparison of the physical properties of each. This will provide new insight into the behavior of the cluster constituents (gas, galaxies, & DM) during a major merger. For example, it is well established that galaxy clusters play an
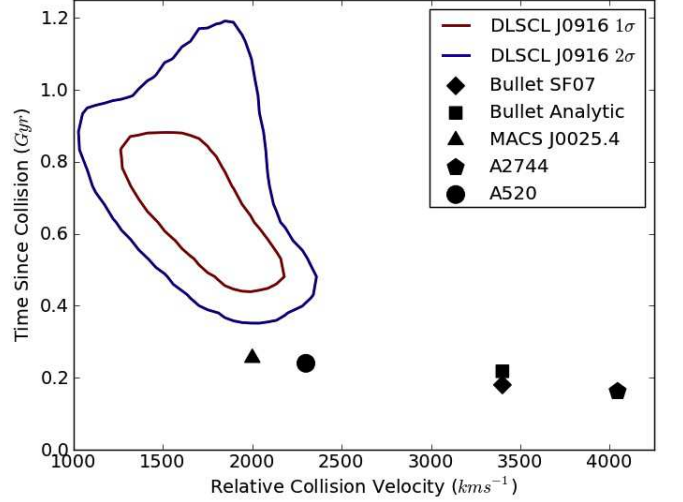

Fig. 4.— The phase space of DLSCL J0916.2+2951 calculated from a Monte Carlo analytical treatment of the system assuming the clusters to be uniform-density spheres with R_{200} radii. The measured velocities of the other mergers (with the exception of "Bullet SF07"; Bradač et al. 2008; Markevitch et al. 2005; Springel & Farrar 2007; Merten et al. 2011) were input into the model to calculate their time-since-collision. It is clear that DLSCL J0916.2+2951 probes a significantly different epoch from the existing dissociative mergers. The close agreement between our analytic estimate, "Bullet Analytic", and the N-body simulation (Springel & Farrar 2007), "Bullet SF07", lends confidence to the results of our analytical treatment.

important role in the evolution of their member galaxies, but it is still unclear whether cluster mergers trigger star formation (e.g. Miller & Owen 2003; Owen et al. 2005; Ferrari et al. 2005; Hwang & Lee 2009), quench it (Poggianti et al. 2004), or have no immediate effect (Chung et al. 2010). This cluster, with its estimated time-since-collision approximately equal to the lifetime of A-stars, holds promise for discriminating between slow-working processes (e.g. galaxy harassment or strangulation) and fast-acting process (e.g. ram pressure stripping).

REFERENCES

Arnaud, K. A. 1996, Astronomical Data Analysis Software and Systems V, 101, 17
Beers, T. C., Flynn, K., & Gebhardt, K. 1990, AJ, 100, 32
Benítez, N. 2000, ApJ, 536, 571
Bertin, E., Mellier, Y., Radovich, M., Missonnier, G., Didelon, P., & Morin, B. 2002, Astronomical Data Analysis Software and Systems XI, 281, 228
Bertin, E. 2006, Astronomical Data Analysis Software and Systems XV, 351, 112
Bradač, M., Allen, S. W., Treu, T., Ebeling, H., Massey, R., Morris, R. G., von der Linden, A., & Applegate, D. 2008, ApJ, 687, 959
Chung, S. M., Gonzalez, A. H., Clowe, D., Markevitch, M., & Zaritsky, D. 2010, ApJ, 725, 1536
Clowe, D., Bradač, M., Gonzalez, A. H., Markevitch, M., Randall, S. W., Jones, C., & Zaritsky, D. 2006, ApJ, 648, L109
Coe, D., Benítez, N., Sánchez, S. F., Jee, M., Bouwens, R., & Ford, H. 2006, AJ, 132, 926
Coil, A. L., et al. 2010, arXiv:1011.4307
Davis, M., et al. 2003, Proc. SPIE, 4834, 161
Diaferio, A., Schindler, S., & Dolag, K. 2008, Space Sci. Rev., 134, 7
Duffy, A. R., Schaye, J., Kay, S. T., & Dalla Vecchia, C. 2008, MNRAS, 390, L64
Fahlman, G., Kaiser, N., Squires, G., & Woods, D. 1994, ApJ, 437, 56
Ferrari, C., Benoist, C., Maurogordato, S., Cappi, A., & Slezak, E. 2005, A&A, 430, 19
Evrard, A. E., Bialek, J., Busha, M., et al. 2008, ApJ, 672, 122
Fischer, P., & Tyson, J. A. 1997, AJ, 114, 14
Gal, R. R., Lemaux, B. C., Lubin, L. M., Kocevski, D., & Squires, G. K. 2008, ApJ, 684, 933
Geller, M. J., Dell'Antonio, I. P., Kurtz, M. J., Ramella, M., Fabricant, D. G., Caldwell, N., Tyson, J. A., & Wittman, D. 2005, ApJ, 635, L125
Gelman, A. & Rubin, D. B. 1992, Statistical Science, 7, 457
Hennawi, J. F., & Spergel, D. N. 2005, ApJ, 624, 59
Hwang, H. S., & Lee, M. G. 2009, MNRAS, 397, 2111
Ilbert, O., et al. 2006, A&A, 457, 841
Kalberla, P. M. W., Burton, W. B., Hartmann, D., et al. 2005, A&A, 440, 775

Jee, M. J., Blakeslee, J. P., Sirianni, M., et al. 2007, PASP, 119, 1403
Jee, M. J., & Tyson, J. A. 2009, ApJ, 691, 1337
Lee, J., & Komatsu, E. 2010, ApJ, 718, 60
Lemaux, B. C., et al. 2009, ApJ, 700, 20
Mahdavi, A., Hoekstra, H., Babul, A., Balam, D. D., & Capak, P. L. 2007, ApJ, 668, 806
Markevitch, M., Gonzalez, A. H., Clowe, D., Vikhlinin, A., Forman, W., Jones, C., Murray, S., & Tucker, W. 2004, ApJ, 606, 819
Markevitch, M., Govoni, F., Brunetti, G., & Jerius, D. 2005, ApJ, 627, 733
Mastropietro, C., & Burkert, A. 2008, MNRAS, 389, 967
Merten, J., Coe, D., Dupke, R., et al. 2011, MNRAS, 417, 333
Miller, N. A., & Owen, F. N. 2003, AJ, 125, 2427
Muchovej, S., et al. 2011, ApJ, 732, 28
Okabe, N., Bourdin, H., Mazzotta, P., & Maurogordato, S. 2011, ApJ, 741, 116
Okabe, N., & Umetsu, K. 2008, PASJ, 60, 345
Ouchi, M., et al. 2004, ApJ, 611, 660
Owen, F. N., Ledlow, M. J., Keel, W. C., Wang, Q. D., & Morrison, G. E. 2005, AJ, 129, 31
Poggianti, B. M., Bridges, T. J., Komiyama, Y., et al. 2004, ApJ, 601, 197
Poole, G. B., Fardal, M. A., Babul, A., McCarthy, I. G., Quinn, T., & Wadsley, J. 2006, MNRAS, 373, 881
Randall, S. W., Markevitch, M., Clowe, D., Gonzalez, A. H., & Bradač, M. 2008, ApJ, 679, 1173
Ricker, P. M., & Sarazin, C. L. 2001, ApJ, 561, 621
Ragozzine, B., Clowe, D., Markevitch, M., Gonzalez, A. H., & Bradac, M. 2011, arXiv:1111.4983
Schindler, S., & Mueller, E. 1993, A&A, 272, 137
Springel, V., & Farrar, G. R. 2007, MNRAS, 380, 911
Steigman, G. 2008, J. Cosmology Astropart. Phys., 10, 1, 10, 1
van Weeren, R. J., Röttgering, H. J. A., Brüggen, M., & Hoeft, M. 2010, Science, 330, 347
Wittman, D. M., et al. 2002, Proc. SPIE, 4836, 73
Yagi, M., Kashikawa, N., Sekiguchi, M., Doi, M., Yasuda, N., Shimasaku, K., & Okamura, S. 2002, AJ, 123, 66